Arch. Metall. Mater. **64** (2019), 4, 1441-1448

DOI: 10.24425/amm.2019.130111

T. KIK*#, J. MORAVEC**, I. NOVAKOVA**

NUMERICAL SIMULATIONS OF X22CrMoV12-1 STEEL MULTILAYER WELDING

The aim of this paper is to present the procedure test for calibration and validation of the numerical model for X22CrMoV12-1 steel multilayer welding. On the real multilayer weld was described how to arrange the whole experiment in order to obtain not only relevant input data but also verification data. Tests on a specially prepared specimen, welded with 8 beads in 4 layers, allows to determine the actual geometry of the single welded beads, registration of welding thermal cycles and the hardness distribution in successively deposited beads together with determining the heat influence of subsequent layers. The results of the real welding tests were compared with the results obtained from the numerical simulations and extended by the calculated stresses and distortions distributions of the tested specimen. A new, improved hardness prediction algorithm for high-alloy martensitic and bainitic steels was also proposed.

Keywords: Keywords: numerical simulation, X22CrMoV12-1, welding, SYSWELD, hardness prediction

1. Introduction

The energy sector is currently the main industrial sector responsible for continuous and dynamic industrial development. Ecological requirements mean that we are still looking for new, better and more ecological electricity production method. Despite huge investments in alternative sources of electricity, still the most strategic are production of electricity from coal (coal steam power plants) and nuclear fusion reaction (nuclear power plants) [1-3].

Although at present it is mainly aimed at closing nuclear and coal-fired power plants, in 2017, about 400 nuclear power plants produced about 25% of the electricity demand of countries in which they are installed in more than 30 countries [1,2]. In an atomic reactor, the heat of the atomic fusion reaction produces steam, which is then transported to the turbines to produce the electricity. This process is very efficient and from one fuel rod (size of a pencil eraser) it is possible to produce energy comparable to that resulting from burning 480 m^3 of natural gas, almost one ton of coal or 560 litres of oil [4]. In addition, without any pollution emitted to the atmosphere. This type of energy also does not degrade the natural environment as well as "ecological" wind turbines or hydroelectric dams. However, people's concerns about radiation cause that we also focus on the second, mentioned type of power plants. The increase in the efficiency of power equipment in the coal-fired power plants also makes it possible to increase their attractiveness to those used so far. Presently most popular are supercritical coal power plants which are working on the steam pressure around 25-28 MPa and the steam temperature reaches approx. 600°C. Their efficiency is about 46%. However, this is not the end of the possibilities. Modern ultra-supercritical power plants work with the pressure of the fresh steam about 37.5 MPa and the temperature reaching 700°C (with efficiency close to the 50%). However such improvement of efficiency is limited by the properties of construction materials that are used [1-4].

In order to ensure a high level of security in the case of modern energy production methods with high parameters as well as high reliability of constructed installations, it is necessary to ensure the highest quality requirements used for their production materials. Among these materials which have a potential for further improvement of processing parameters are the martensitic 9-12% Cr steels. These steels offer a very good combination of strength properties, resistance against high-temperature oxidation and creep, low price and good processability [4-10]. However, it is also important to take into account the problems encountered in welding these materials. Steels used in nuclear energy have a problems related with tendency to cold cracking, hydrogen embrittlement and very often require complicated preheating and post weld heat treatment operations [5-10].

Due to the specificity of technology and the degree of advancement of materials and technologies to combine them, it is also important to conduct research on their properties change during the manufacturing processes. One of such processes that significantly change the properties of the material is the welding process [8-14]. The degree of complexity of the ma-

* SILESIAN UNIVERSITY OF TECHNOLOGY, DEPARTMENT OF WELDING ENGINEERING, 18A KONARSKIEGO STR., 44-100 GLIWICE, POLAND
** TECHNICAL UNIVERSITY OF LIBEREC, DEPARTMENT OF ENGINEERING TECHNOLOGY, LIBEREC, CZECH REPUBLIC
# Corresponding author: tomasz.kik@polsl.pl

chine elements and construction produced by this technology causes that more and more often we must use the possibilities offered by today's modern software for numerical analyses of welding and heat treatment processes. This type of software allows for a significant extension the possibilities of designing modern power installations by providing engineers with a lot of important information about both the process itself and its effects. Significant reduction of the number of tests necessary to run on real samples as well as often inability to perform them due to the dimensions and weight of the structure gives unprecedented possibilities to design modern power installations, at the same time with very significantly reduced financial outlays [4,8,14-19].

2. The range of studies

The purpose of the presented research was to determine the conditions for conducting a suitably prepared experiment allowing to obtain input data for calibration and validation of the numerical calculation model and then also to calculate the stress and strain distribution in simulated multi-pass welding. For this purpose, a sample of X22CrMoV12-1 steel with dimensions of 180×80×20 mm was prepared in which a groove 12 mm wide, 10 mm deep and an angle of 30° was milled in the middle part, Fig. 1.

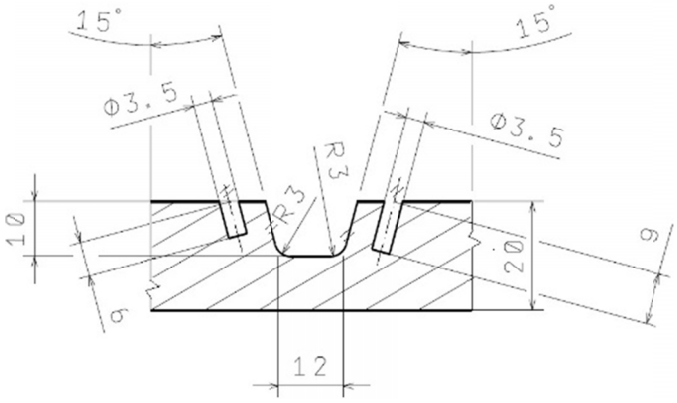

Fig. 1. The shape and dimensions of the test specimen at the cross-section

Chemical composition of X22CrMoV12-1 steel measured on TASMAN Q4 spectrometer was shown in Table 1. As a filler material, Thermanit MTS 4 EN ISO 3580-A E CrMoWV12 B 4 2 H5 coated electrode with a diameter 2,5 mm and a total length 250 mm was used – Table 2.

The main aim of real tests was not to achieve the best quality of welds but collect as more as it possible of input data for numerical simulations. The obtained input data were used to determine the boundary conditions as well as for the verification of the calculated results. They were mainly: microsection views, recorded thermal cycles and hardness distribution after welding and post weld heat treatment. A welding jig was made whose supporting structure consists of 50 mm thick cast iron plate which is able to transfer heat to the tested specimen during the welding test, Fig. 2. Moreover, this plate is equipped with grips to fix the welded part. Due to that, there is possible to accurately define a place and clamping stiffness – thus relevant simulation computation boundary condition. Test specimen were monitored by six thermocouples partially coated with Sibral (aluminosilicate) isolation. The specimen was clamped into a mentioned jig placed into the furnace and heated on temperature 250°C. After reaching preheating temperature on the whole specimen, Sibral isolation was placed also on the top to eliminate heat loss due to radiation. During all welding procedure, the interpass temperature at 300°C was respected. The complete specimen was welded by MMAW method with 8 beads in 4 layers, where two beads were placed side-by-side in each layer. In order to determine the geometry of individual beads, every subsequent layer has its origin offset by 25 mm towards the previous layer. The welding process was completely monitored by the WeldMonitor system to monitor the correctness of the parameters used. Because the MMAW method is characterized by considerable variability of parameters, the average value of parameters for analysis were as follows: welding current 75 A, arc voltage 23 V, welding speed about 2.2 mm/s. After finishing the welding process the isolation was removed and the tested specimen was cooled down to the ambient temperature. Thermocouples were welded to the test specimen in several, selected locations at different depths (from 0 to 9 mm from the sample surface) to obtain more precise information on the thermal cycle of the welding process, Fig. 2.

TABLE 1

Chemical composition of X22CrMoV12-1 steel measured on TASMAN Q4 spectrometer, %

C	Mn	Si	P	S	N	Cu	Ni	Cr
0.206	0.682	0.246	<0.005	<0.15	0.037	0.092	0.626	11.7
V	Al	W	Ti	Nb	As	Mg	Fe	Mo
0.337	0.014	<0.01	0.0019	0.011	0.011	0.012	84.81	0.825

TABLE 2

Chemical composition of Thermanit MTS 4 EN ISO 3580-E CrMoWV12 B 4 2 H5 covered electrode, %

C	Mn	Si	W	V	N	Nb	Ni	Cr	Mo
0.18	0.6	0.3	0.5	0.3	—	—	0.6	11.0	1.0

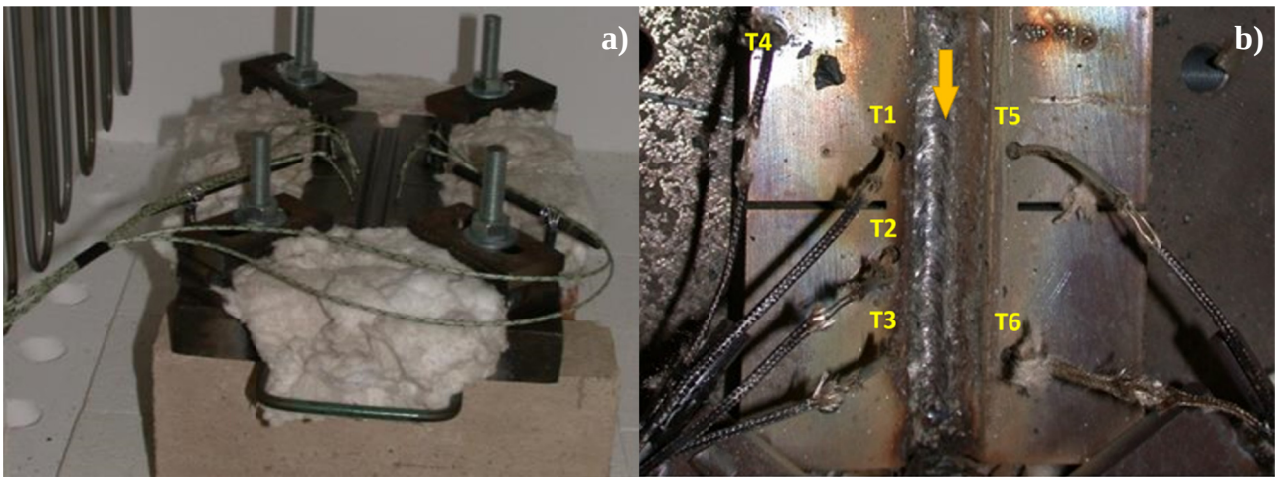

Fig. 2. View of the sample before welding placed in the furnace a) and after the welding process with visible thermocouples b)

3. Numerical simulations and welding experiments

To make numerical calculations possible, it was necessary to create a material model of X22CrMoV12-1 steel in the software based on the finite element method (SYSWELD environment). For this purpose, Gleeble 3500 thermo-mechanic physical simulator was used. Based on the tests, it was possible to create a CCT diagram and obtain data necessary to build a complete material database. Due to the minimal differences in the chemical composition, the constructed material base was also used in the simulation for the consumable definition. Next, a three-dimensional numerical finite element (FE) model was created, on the basis of the macrostructure research results with the real geometry of every deposited bead, Fig. 3.

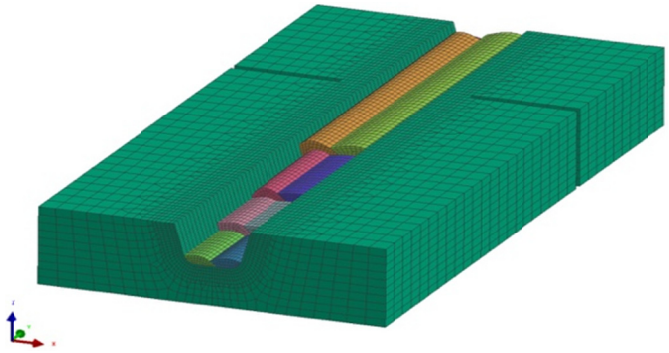

Fig. 3. View of a 3D numerical model of a weld created on the basis of real experiment geometry

The mechanical boundary conditions were set in the corners of the sample as corresponding to the real clamps in the experiment. In numerical model they were implemented by a flexible boundary condition with high stiffness (10 kN/mm per node). In order to simulate contact with the heating plate, a simple boundary condition limiting the feed (also stiffness 10 kN/mm per node) in the direction perpendicular to the bottom wall of the sample was used, because the deflection was found to be practically zero towards the heating plate. Therefore, the use of contact is not necessary, since only a slight offset of the welded plate from the heating plate occurs. The boundary conditions associated with the sample cooling are for the heat transfer through the bottom of the sample to the heating plate, where the heat transfer coefficient corresponds to the metal-metal contact and is about 0.002 W/mm^2×K and the heat sink into the environment by SIBRAL insulation represented by the corresponding low heat transfer coefficient at 1.5×10^{-5} W/mm^{2}K. The simulation was carried out as a transient simulation.

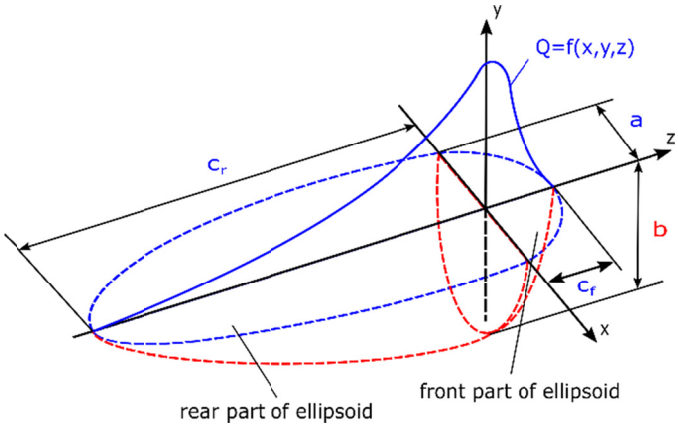

Fig. 4. Double ellipsoid heat source model [13]

As a heat source model, the double-ellipsoidal model (also called Goldak's model) of heat source was used, Fig. 4. Transferred heat is described by the equations below [18,19].

For the front part of the heat source model, it can be described as Eq. (1):

$$Q_f(x,y,z)=\frac{6\sqrt{3}f_f Q}{abC_f\pi\sqrt{\pi}}\exp\left(\frac{-3x^2}{a^2}\right)\exp\left(\frac{-3y^2}{b^2}\right)\exp\left(\frac{-3z^2}{c^2}\right) \quad (1)$$

and, for the rear part of the heat source model, it can be described as Eq. (2):

$$Q_r(x,y,z) = \frac{6\sqrt{3} f_r Q}{abC_r \pi \sqrt{\pi}} \exp\left(\frac{-3x^2}{a^2}\right) \exp\left(\frac{-3y^2}{b^2}\right) \exp\left(\frac{-3z^2}{c^2}\right) \quad (2)$$

where: Q_f, Q_r – heat introduced into the front and the rear part of the model, Q – total power source, a – width of the molten pool, b – the depth of the molten pool, c_f, c_r – length of the front and the rear part of the molten pool, f_f, f_r – constants which influence energy flow intensity into the material.

The efficiency of the heat transfer into the welded material is given by the applied welding method. The geometry of the double-ellipsoidal model can be modified by changing coefficients a, b, and c contained in the equations. It is important that SYSWELD enables the capability to introduce a power density function applied to the structure Q_R (W/mm^3). Because of it, the energy is divided into O_f and Q_r values. The first value is the heat energy density in the front half of the ellipsoid (maximum source frontal intensity), and the second is that in the rear part (maximum source rear intensity), Fig. 4. Total energy introduced by the heat source model to the welded material is Eq. (3) [18,19]:

$$P = \int_{structure} Q_R \quad (3)$$

Calibration of the heat source model was carried out for each bead separately and the obtained temperature fields were compared with the results of macroscopic studies, Fig. 5. To properly capture the shape of the molten areas, a limitation of the source function to the mesh of individual beads has been applied, so that the heat spreads through conduction to the surrounding base material. To ensure correct melting of individual bead areas, the specific parameters of the heat source model shape were determined as: a = 15 mm, $c_f + c_r$ = 6 mm, b = 2 mm, Fig. 4.

3.1. Welding thermal cycles

The acquisition of welding thermal cycles using thermocouples also allows obtaining input data to the computational model. The comparison of thermal cycles registered in actual welding trials with cycles calculated in grid nodes corresponding to the placement of the thermocouples allows, in addition to comparing the geometry of the melted area, to a precise calibration and also validation of the proposed calculation model, Fig. 6 and 7. The individual beads were welded from up to three parts (to change the electrode), so in some cases, more than one maximum temperature for each thermocouple is recorded in the diagrams, Fig. 6.

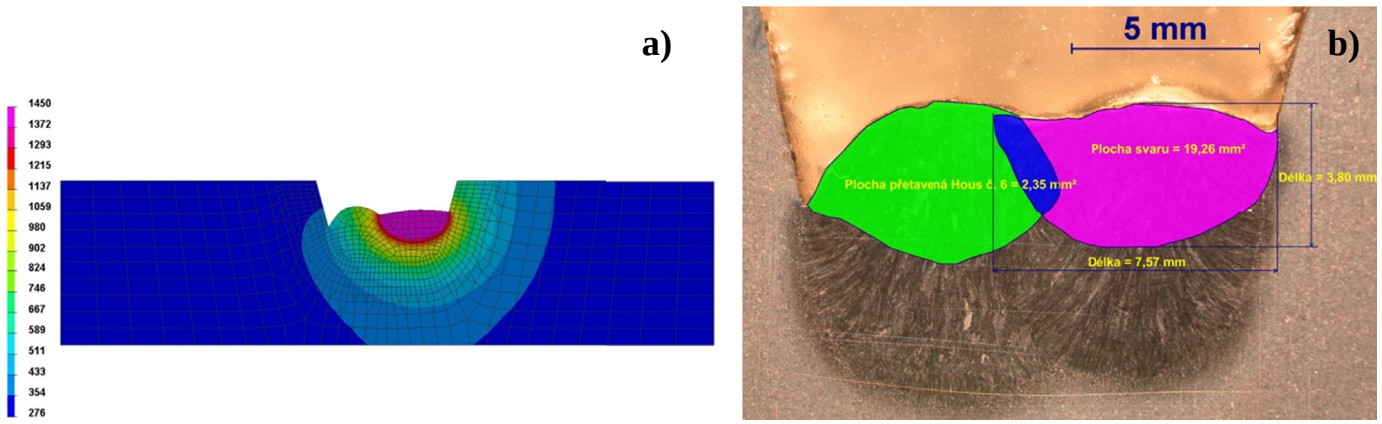

Fig. 5. A calibration example of the heat source model for bead number 4 – view of the temperature distribution on the cross-section of the model a) and geometry of 3rd and 4th bead b)

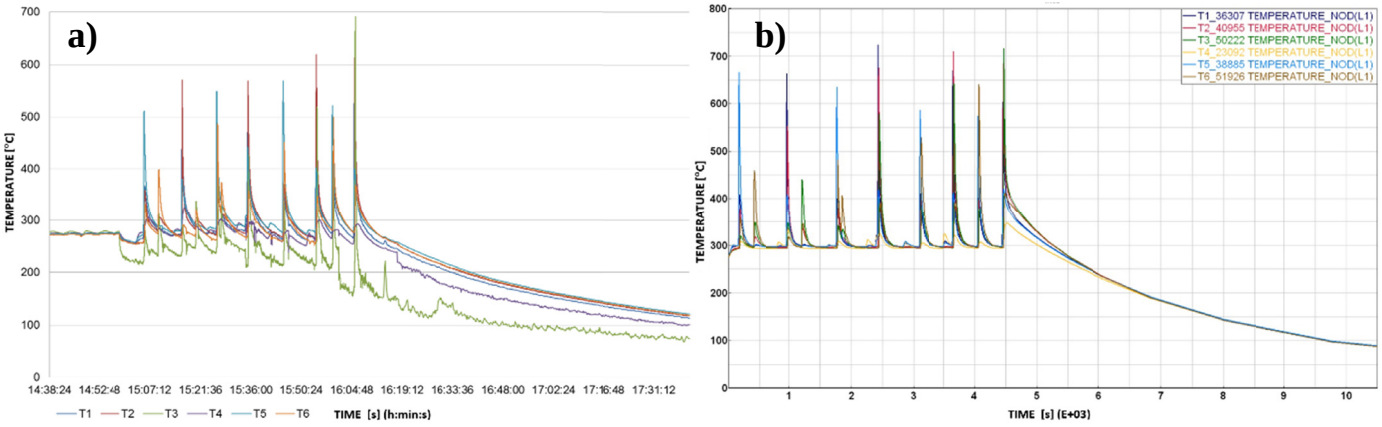

Fig. 6. Registered a) and calculated b) thermal cycles for all six thermocouples during the complete welding process

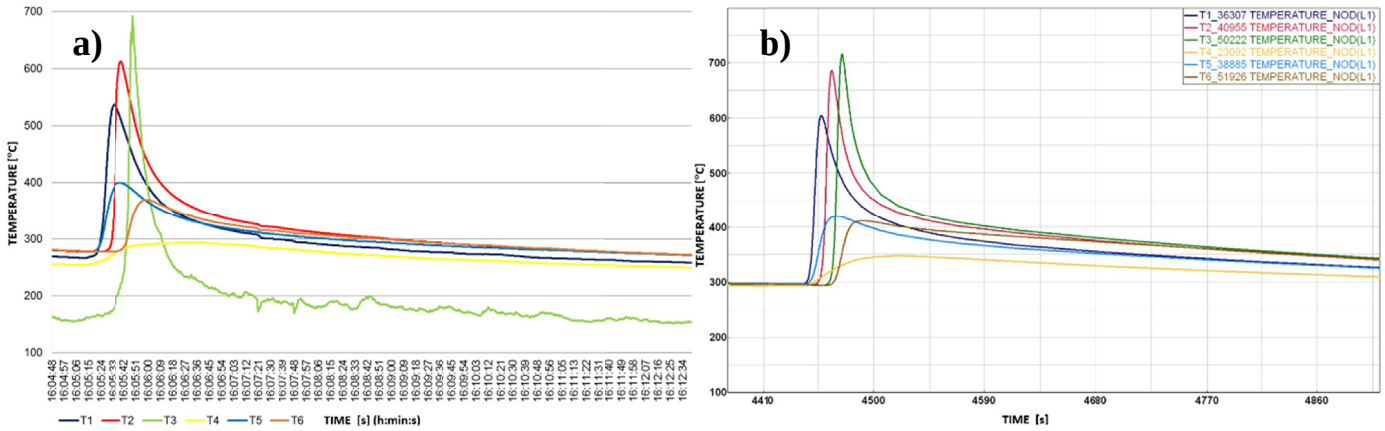

Fig. 7. Comparison of registered a) and calculated b) thermal cycles for all six thermocouples during 8th bead welding

3.2. Metallurgical phases distribution

The whole process calculated in SYSWELD consists of two analyses – the thermo-metallurgical and the mechanical one. The first analysis makes it possible to compute non-stationary temperature fields, phase transformations, hardness or size of the austenitic grain. The mechanical analysis uses the results of the temperature-metallurgical analysis as input data and the most common results here are mainly stress and strain fields. The calculations of the metallurgical phase distributions carried out on the model described showed the occurrence of a martensitic structure in the whole weld volume with a small proportion of the bainitic structure near the area under the sample groove. This was also confirmed by the results of metallographic and hardness measurements, Fig. 8.

3.3. Hardness distribution

Hardness was measured from the parent material across HAZ to weld metal and then again across HAZ always to the parent material. All rows of measurement points were on the individual cross sections made always in the same place so it was possible to monitor the influence of individual thermal cycle runs on the change of hardness in relevant places. A series of hardness measurements were made on each section such that the first row was placed 6 mm from the bottom edge of the sample and each subsequent row was moved up by 2 mm. It means that the first row was placed across not HAZ and row 2 goes through HAZ on a lower edge of beads 1 and 2 as is shown in Fig. 9. Successive rows (from 3 to 6) pass from the base material, through the HAZ and the weld. By using this proposed measurement method, it is possible to describe the influence of such thermal treatment on

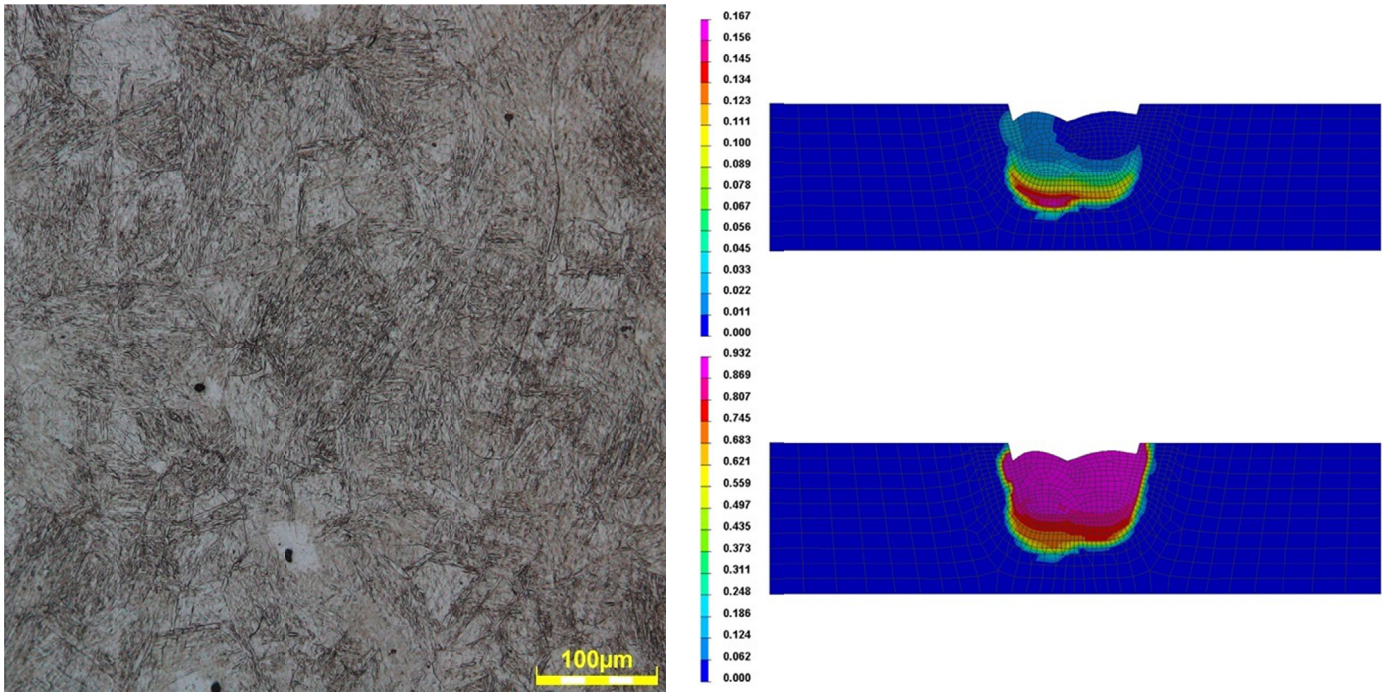

Fig. 8. A view of martensitic microstructure of tested weld and results of metallurgical phases calculations (bainite distribution at the top and martensite distribution at the bottom)

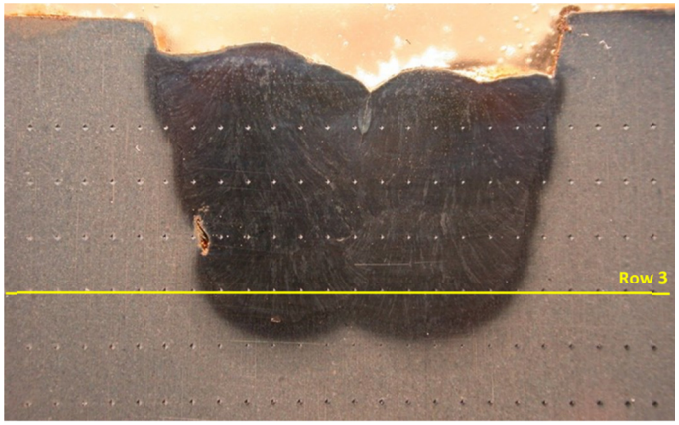

Fig. 9. Macrostructure of the area with eight beads with visible six hardness measurement rows

the final hardness of structure by hardness measurement in the tempered part of the welded joint.

The results of hardness measurements on the cross-sections of the tested samples for each deposited layer were compared separately with the results of calculated hardness in the numerical simulations. Particular differences in the calculated and measured values were observed in the case of the sample after the tempering process. Hence, the data obtained as a result of the research served to develop a new hardness prediction model.

The numerically calculated structural analysis which was carried out on the basis of temperature fields calculations by means of Goldak's model detected martensite structure with a low portion of bainite – mainly in HAZ [4,18]. The equation used for hardness calculation of the martensitic phase was Eq. (4):

$$HVM = 127 + 949C + 27Si + 11Mn + \\ + 8Ni + 16Cr + 21Log10(V_r) \quad (4)$$

bainite phase was calculated from the Eq. (5):

$$HVB = -323 + 185C + 330Si + 153Mn + 65Ni + \\ + 144Cr + 191Mo + Log10(V_r) \times \\ \times \begin{pmatrix} 89 + 53C - 55Si - 22Mn - 10Ni + \\ - 20Cr - 33Mo \end{pmatrix} \quad (5)$$

and hardness calculation after tempering was calculated from Eq. (6) and Eq. (7):

$$HVTemp = -74 - 434C - 368Si + 15Mn + 37Ni + \\ + 17Cr - 335Mo - 2235V + (103/p) \times \\ \times \begin{pmatrix} 260 + 616C + 321Si - 21Mn + \\ - 35Ni - 11Cr + 352Mo + 2345V \end{pmatrix} \quad (6)$$

$$p = \left(\frac{1}{T_p} - \frac{R}{\Delta H} \cdot \ln t_p \right)^{-1} \quad (7)$$

where: V_r – cooling rate [°C/s], 'p' – tempering parameter given by tempering temperature T_p [°C], ΔH – change of activation energy [J/kg], t_p – tempering time [s] and R – gas constant [J/mol×K].

The use of the new hardness calculation formula compared to the older standard implemented in SYSWELD slightly changes the results obtained after the welding process simulation. However, the calculation of heat treatment after welding (tempering) shows a significant advantage of the new model, which is much more efficient in predicting the hardness for this type of materials, Fig. 10 and 11. The following figures show the comparison of the hardness of the selected measuring line (row 3) for simulations and for the experiment, Fig. 10. The individual curves correspond with their colours.

3.4. Stresses and distortions distribution

On the basis of the thermo-metallurgical calculations, SYSWELD also allows calculating the distribution of mechanical properties taking into account the influence of metallurgical transformations and the welding thermal cycles. Due to the nature of the experiment and the lack of measurements of stresses and distortions of the welded sample, it is not possible to compare the presented simulation results directly with the results of the experiment, Fig. 12 to 14. However, in the case of numerical analyses, they constitute a very important source of information about the whole welding process and the heat input of individual beads on changes in welded materials.

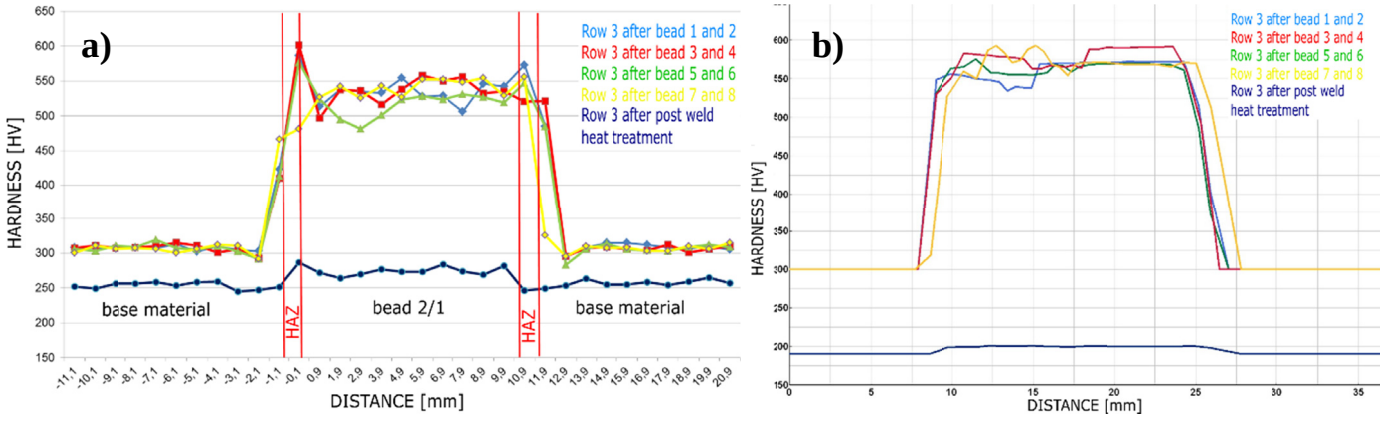

Fig. 10. Vickers hardness distribution in Row 3 – values from the experiment a) and calculated b)

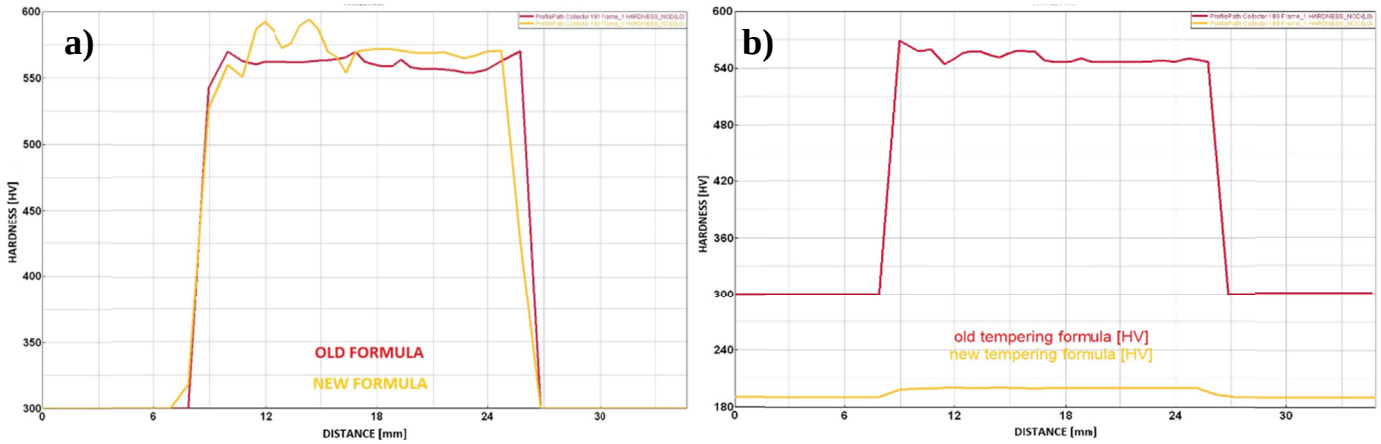

Fig. 11. Comparison of an old and new formula for hardness calculation – after welding a) and tempering b)

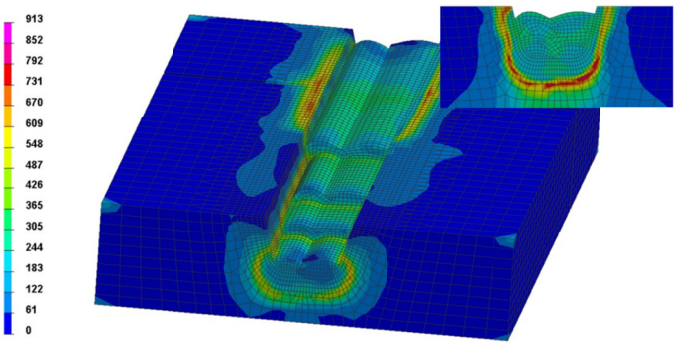

Fig. 12. Reduced stresses (von Mises) distribution after welding – 3D view and cross-section in the area of all 8 beads

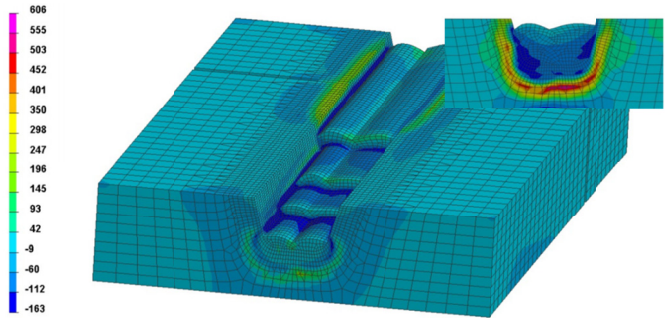

Fig. 13. Mean stresses distribution after welding – 3D view and cross-section in the area of all 8 beads

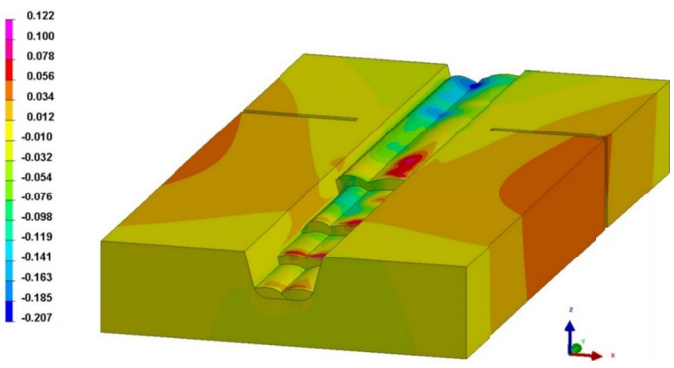

Fig. 14. Distortions distribution after welding (in Z-axis direction – vertical)

4. Summary

On the basis of the conducted tests, calibration and verification of the numerical model of the multi-layer welding process of the X22CrMoV12-1 steel sample were carried out. The proposed way of layers deposition on a real sample, allowed to determine the exact geometry of the obtained beads. Calibration of the heat source model based on the actual geometrical dimensions and the shape of the single beads performed made it possible to precisely determine its parameters and obtain high compliance with the actual welding tests. This was confirmed by the comparison of registered and calculated welding thermal cycles. Generally, the calculated temperature curves at the measuring points in the thermocouple locations correspond very well to the experiment's output values. The only exception is the T3 thermocouple, in which the values from the simulation and the experiment differ significantly, but rather can be attributed to a measuring problem, for example, incorrect connecting of the thermocouple to the tested sample. This conclusion was formulated based on a comparison of the recorded values with the record from the other thermocouples and own experiences of the authors. In addition to the incorrect mounting of the thermocouple tip, is also possible in the case of the proposed measurement methodology, when the thermocouple is inaccurately positioned in the measuring hole – an example of small discrepancies in the results for the T2 thermocouple – probably placed at the wrong depth.

A specially designed experiment also allowed to perform hardness measurements in such a way that it was possible to determine the heat impact of each subsequent layer on changes in hardness distributions on the cross-section of the tested sample. Hardness calculations were carried out in accordance with the standard methodology implemented in SYSWELD and the newly proposed formula. The calculated and measured hardness values after welding are basically the same, the experimental values in the weld area are only slightly lower. But also an interesting relationship was noticed. Comparison of the results of hardness calculations after welding according to the older type of formula showed very close data to real values. It can, therefore, be

concluded that both the old and the newly proposed calculation approach lead to similar results. Nevertheless, it can be said that in areas where after welding there is a certain amount of bainite in the microstructure of the material (lower parts of the joint being made), the new formula allows for better mapping of the actual values. However, the use of the old formula for calculating the heat treatment process (in this case the tempering process) leads to completely unrealistic results. In this situation, the old hardness prediction model does not fully reflect the specificity of the heat treatment after the welding process. It is very well visible on the graph of the results of numerical analysis, where for the case of using the old formula, the values in the area of the weld and HAZ are still high, Fig. 11. The new formula significantly improves the consistency of results, despite the differences between the results of calculations lower by about 50 HV compared to those obtained experimentally.

The performed analyses of stress and strain distribution of the sample also indicate the level of values that seem to confirm the occurrence of a martensitic structure, ascertained by the calculations of the distributions of metallurgical structures and hardness measurements.

In conclusion, because in the case of high-alloy martensitic and bainitic steels, it is difficult to clearly determine the effect of individual alloying elements on substitution reinforcement of a solid solution and also precipitations with different thermodynamical stability, proposed new equations which will be suitable for hardness calculations on tempering for martensitic and bainitic chromium steels. These equations taking into consideration mainly structure hardness before tempering, the influence of tempering temperature and heating time. It should be noted that the presented research and the creation of a new computational hardness model for the X22CrMoV12-1 steel material test database have increased the usability of the software.

REFERENCES

[1] https://www.nei.org/news, accessed: 10.05.2019.

[2] http://www.world-nuclear.org/information-library/country-profiles/countries-t-z/usa-nuclear-power-policy.aspx, accessed: 10.05.2019.

[3] http://www.nrc.gov/reading-rm/doc-collections/fact-sheets/power-uprates.html, accessed: 10.05.2019.

[4] J. Moravec, T. Kik, I. Novakova, Application of numerical simulations on X10CrWMoVNb9-2 steel multilayer welding, MM Science Journal **11**, 1190-1193 (2016), doi: 10.17973/MMSJ.2016_11_201628.

[5] A. Świerczyńska, J. Łabanowski, J. Michalska, D. Fydrych, Corrosion behavior of hydrogen charged super duplex stainless steel welded joints. Materials and Corrosion **68** (10), 1037-1045 (2017).

[6] K. Pańcikiewicz, Structure and properties of welded joints of 7CrMoVTiB10-10 (T24) steel, Advances in Materials Science **18**, 1, 37-47 (2018).

[7] C. Pandey, M.M. Mahapatra, P. Kumar, J.G. Thakre, N. Saini, Role of evolving microstructure on the mechanical behaviour of P92 steel welded joint in as-welded and post weld heat treated state, Journal of Materials Processing Technology **263**, 241-255 (2019).

[8] J. Moravec, I. Novakova, J. Sobotka, T. Kik, Application possibilities of the low-temperature repairs on creep-resistance turbine components from material GX23CrMoV12-1, MATEC Web of Conferences, Volume 244, 5 December 2018, Article number 01017 (2018).

[9] D. J. Abson, J. S. Rothwell, B. J. Cane, Advances in welded creep resistant 9-12%Cr steels, 5th International Conference on Advances in Materials Technology for Fossil Power Plants, Marco Island, FL, United States, October, (2007).

[10] J. Hald, Development status and future possibilities for martensitic creep resistant steels, Materials for Advanced Power Engineering, pp. 55-66 (2010).

[11] J. Tomków, G. Rogalski, D. Fydrych, J. Łabanowski, Advantages of the Application of the Temper Bead Welding Technique During Wet Welding. Materials **12** (6), 915 (2019).

[12] R. Bęczkowski, Repair welding of the massive cast, Archives of Foundry Engineering **17** (2), 5-8, 2017.

[13] T. Chmielewski, D. Golański, The role of welding in the remanufacturing process, Welding International **29**, 11, 861-864 (2015).

[14] J. Winczek, K. Makles, M. Gucwa et al., Modelling of Strains During SAW Surfacing Taking into Heat of the Weld in Temperature Field Description and Phase Transformations, International Conference on Materials, Alloys and Experimental Mechanics (ICMAEM-2017) Book Series: IOP Conference Series-Materials Science and Engineering,Vol.: 225, Article Number: 012038 Published: 2017.

[15] A. Sajek, Application of FEM simulation method in area of the dynamics of cooling AHSS steel with a complex hybrid welding process, Welding in the World **63**, 4, 1065-1073 (2019).

[16] T. Richter, M. Slovacek, J. Tejc, Materials models – numerical prediction of hardness, yield strength and ultimate strength, Tech. report M_Z_13_023_r01, Mecas ESI, Plzen (2013).

[17] S. Joshi, S. Hildebrand, A. Aloraier, T. Rabczuk, Characterization of material properties and heat source parameters in welding simulation of two overlapping beads on a substrate plate. Computational Materials Science **69**, 559-565 (2013).

[18] T. Kik, M. Slovacek, Numerical simulation of welding plates from material X10CrWMoVNb 9-2, Technical report M_Z_13_020_r01, Mecas ESI, Plzen (2013).

[19] Sysweld manual ESI Group, Welding Simulation User Guide; ESI Group, France, (2016).